Nucleation of Ligand-Receptor Domains in Membrane Adhesion

Timo Bihr,[1] Udo Seifert,[1] and Ana-Sunčana Smith[2]

[1]*II. Institut für Theoretische Physik, Universität Stuttgart, Pfaffenwaldring 57, 70550 Stuttgart, Germany*
[2]*Institut für Theoretische Physik and the Excellence Cluster: Engineering of Advanced Materials, Universität Erlangen-Nürnberg, Nägelsbachstrasse 49b, 91052 Erlangen, Germany*

(Received 11 May 2012; published 19 December 2012)

We present a comprehensive model for the nucleation of domains in membrane adhesion. We determine the critical number of bonds in a nucleus and calculate the probability distribution of nucleation time from a discrete master equation. The latter is characterized by only four effective rates, which account for cooperative effects between bonds. We validate our model by finding excellent agreement with extensive Langevin simulations. In the range of parameters typical for cell adhesion, we find the critical number of bonds to be small. Furthermore, we find a characteristic separation between the bonds at which nucleation is particularly fast, pointing to potential regulatory mechanisms that could be used to control the cell recognition processes.

DOI: 10.1103/PhysRevLett.109.258101 PACS numbers: 87.16.D−, 87.15.kp, 87.16.A−

Cell adhesion is mediated by domains consisting of ligand-receptor bonds connecting either two cells or a cell with the extracellular environment. As key elements in the machinery of the cell recognition and mechanosensing [1], domains are implicated in up and down regulation of a number of processes [2] including determining the morphology [3] and protein expression [4] of stem cells, immunological response [5], cell differentiation [6], or the control of homeostatic pressure in tissues [7,8].

Adhesion domains are commonly studied on relatively long time and length scales, whereby the overall adhesion is sensitive to the density of immobilized binders and to the stiffness of the substrate [9,10]. This sensitivity was also reflected in the structure of the actin cortex [11] and the ability of cells to generate forces [12]. These forces were found to act on adhesion domains, rendering them unstable in all but a narrow range of sizes [10,13].

Much of the current understanding of the formation of domains arises from studies of vesicles specifically binding to a substrate (for reviews, see Refs. [14,15]). Thereby, domains form spontaneously, with densely packed ligand-receptor bonds [16,17]. However, the stability of bonds at the edge of the domain, as well as the number and the morphology of domains, were found to vary most with the density of binders on the substrate [18,19], reminiscent of observations in the cellular context. These results could be explained by extensive simulations [19–21] and by theoretical modeling of both the adhesion equilibrium [21,22] and the dynamics of growth, typically long after the stable seed of the domain was formed [16,17,23–27].

On the other hand, very little is known about the nucleation stage of domain formation. The related debate has focused upon establishing the size of a stable nucleus, where the seed of a domain was typically predicted to contain a large number of bonds [25,28,29]. However, the resolution of optical microscopes has recently become such that early stages of the domain formation could be studied [13,30]. Consequently, it was suggested that membrane fluctuations play an important role, and that already a few bonds may be sufficient to form a stable seed [31].

The difficulty in modeling the nucleation [32] arises from the coupling of the deformations of the fluctuating membrane and bond association and dissociation rates [19,33]. This coupling induces density dependent correlations [21,34], promotes the formation of bonds, and enhances the stability of already formed bonds [35]. Here, we elucidate the importance of these correlations for the nucleation and arrive at a theoretical prediction for the number of bonds in a stable seed, as well as the characteristic nucleation time. We demonstrate the validity of our approach by achieving a favorable comparison with relevant simulations and available experimental data [18,31]. The related technical formalism is presented in the Supplemental Material [36].

The model.—The membrane is assumed to contain freely diffusing ligands with a concentration of ρ_l. The ligands occasionally form bonds with receptors. The latter are immobilized on the substrate in the concentration ρ_r and modeled as thermalized harmonic springs of stiffness λ and rest length l_0. A bond is created when the distance between the ligand and the receptor is in the range α of a steplike interaction potential, the depth of which is given by the binding affinity of the pair ϵ_b. By considering the entropy cost associated with the change in receptor fluctuations upon bond formation, an effective affinity $\bar{\epsilon}_b = \epsilon_b + k_B T \ln[\lambda\alpha^2/(2\pi)]/2$ is deduced.

The Hamiltonian of the system (Fig. 1) explicitly accounts for the deformation of the fluctuating membrane [34,37] and the bonds [19]. They are both parametrized by the space and time dependent height $h(\mathbf{r}, t)$ of the membrane above the substrate. Hence,

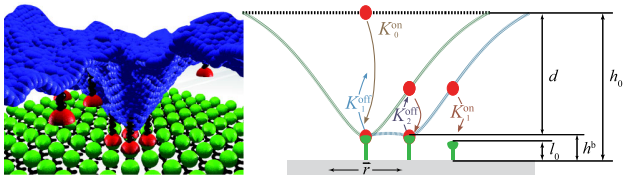

FIG. 1 (color online). Left: Snapshot of a nucleation site from a simulation. Right: Explicitly calculated membrane profiles for a seed with zero (black), one (green), and five (blue) bonds, the shapes of the latter two being nearly identical. Effective rates for the association (K_n^{on}) and the dissociation (K_n^{off}) of bonds in a growing seed are displayed.

$$\mathcal{H}[h(\mathbf{r},t)] = \int_A d^2\mathbf{r}\left\{\frac{\kappa}{2}[\nabla^2 h(\mathbf{r},t)]^2 + \frac{\gamma}{2}[h(\mathbf{r},t) - h_0]^2 + \sum_{i=1}^{N_t(t)} \delta(\mathbf{r} - \mathbf{r_i})\left[\frac{\lambda}{2}(h(\mathbf{r},t) - l_0)^2 - \epsilon_b\right]\right\}. \quad (1)$$

The Helfrich energy (first term) term describes the bending of the membrane in a harmonic potential (second term) of a strength γ with a minimum at h_0 [38]. The latter accounts for the glycocalyx and other implicit potentials (van der Waals, Coulomb, hydration...), whose role is to prevent unspecific contacts and keep the unbound membrane at a relatively large separation from the substrate [39]. The last term sums over the enthalpy of a total of $N_t(t)$ bonds formed at the set of positions $\{\mathbf{r_i}\}$. The entropy change associated with ligand diffusion during nucleation can be neglected.

The critical size of the stable nucleation seed.—In our variant of the capillarity approximation (see Supplemental Material [36]), we calculate the critical number of bonds N_c in the seed by balancing the increase in the free energy due to the membrane deformation and the decrease in binding enthalpy

$$N_c = 1 + \frac{4d^4\rho_r\gamma\sqrt{\gamma\kappa}}{\pi(\gamma d^2 - 2\bar{\epsilon}_b\rho_r)^2}. \quad (2)$$

Thereby, d is the change in height experienced by the membrane (see Fig. 1). Furthermore, we assume that all receptors within the seed are bonded [25,26] and recognize that the membrane profile (Fig. 1) associated with the formation of one bond [34,37] characterizes the shape of the moving edge in a small seed (deformation energy is proportional to the seed circumference).

Notably, N_c diverges when $\gamma d^2 = 2\bar{\epsilon}_b\rho_r$, beyond which specific adhesion is unstable. Because the receptors are immobile and ligands mobile, N_c explicitly depends on ρ_r but not on ρ_l. In the context of cell adhesion, in which active regulation can modify the local binder density, the membrane stiffness, or the glycocalyx, this result points to possible regulatory mechanisms. Under the conditions used in experiments on vesicles [18,31], Eq. (2) correctly predicts stable seeds of 2–4 bonds, depending on the affinity of the ligand-receptor pair in question (Fig. 2).

Nucleation dynamics.—The dynamics of nucleation is often addressed through the concept of the mean first passage time [40]. Thereby, one calculates the time τ for the system to evolve from the state A (no bonds), to the state B (N_c bonds). Depending on the path (the sequence of binding and unbinding events prior to the establishment of the N_cth bond), a distribution $\mathcal{P}(\tau)$ of first passage times emerges, the first moment of which is the mean first passage time or, in our case, the characteristic nucleation time $\bar{\tau}$. The corresponding master equation couples the time variation of all probabilities P_n for finding seeds with $n \leq N_c - 1$ bonds (see Supplemental Material [36]). These probabilities are primarily dependent on rates at which the bonds form and break.

The confinement of the receptors and ligands to opposing surfaces makes the association and dissociation rates, $k^{on}(h)$ and $k^{off}(h)$, dependent on the local instantaneous distance h between the two membrane [41]. By postulating local thermodynamic equilibrium for each receptor, these so-called Dembo's rates satisfy the detailed balance condition

$$\frac{k^{off}(h)}{k^{on}(h)} = \exp\left[\left(\frac{\lambda}{2}(h - l_0)^2 - \bar{\epsilon}_b\right)\right], \quad (3)$$

where we set $\beta \equiv (k_BT)^{-1} \equiv 1$. In the spirit of previous works [19,42,43], we relate k^{on} to the probability of finding a ligand and a receptor within the range of the interaction potential α, averaged over all receptor conformations

$$k^{on}(h) = k_0\sqrt{\frac{\lambda\alpha^2}{2\pi}}\exp\left[-\frac{\lambda}{2}\{(h - l_0) - \alpha\}^2\right]. \quad (4)$$

Thereby, k_0 is the intrinsic reaction rate (the inverse of the attempt frequency). The local unbinding rate k^{off} follows from the detailed balance equation (3) and is explicitly dependent on the effective binding affinity $\bar{\epsilon}_b$.

The time scale k_0^{-1} typical for binding and unbinding of a bond sets the time scale at which a membrane shape-profile associated with a particular configuration of n bond

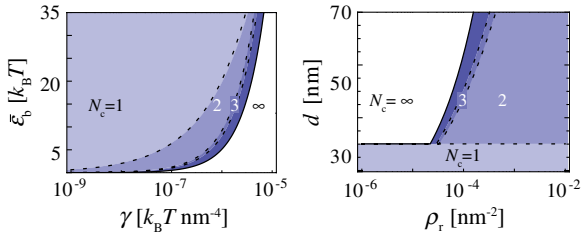

FIG. 2 (color online). Phase diagrams showing regions of unstable adhesion ($N_c = \infty$) and regions with a particular number of bonds forming a stable seed ($N_c = 1, 2, 3, \ldots$) for $\kappa = 10k_BT$ (k_B being the Boltzmann constant and T temperature), $\gamma = 3.125 \times 10^{-7} k_BT$ nm^{-4}, $h_0 = 80$ nm, and $l_0 = 40$ nm, $\epsilon_b = 6.97k_BT$, $\rho_l = 1.5625 \times 10^{-4}$ nm^{-2}, and $\lambda = \infty$. These parameters are used throughout unless otherwise indicated.

is stable. However, membrane fluctuations occur on time scales much shorter than k_0^{-1}. Consequently, the membrane samples the entire height probability distribution p_n, before an existing bond dissociates and a new one associates. The ligands also sample all available heights while attempting to form or break a bond. Simultaneously, rapid changes of $k^{\mathrm{on}}(h)$ and $k^{\mathrm{off}}(h)$ with fluctuations of the membrane take place. Such time-scale separation allows us to perform the key step in the development of our model, namely to define a set of effective rates K_n^{off} and K_n^{on} to break the nth or form the $(n+1)$th bond. These emerge by averaging the local rates $k^{\mathrm{on}}(h)$ and $k^{\mathrm{off}}(h)$ by means of the characteristic distribution p_n

$$K_n^{\mathrm{off}} \equiv \int dh^b\, p_n(h^b) k^{\mathrm{off}}(h^b)$$
$$K_n^{\mathrm{on}} \equiv \rho_l \int dh^r\, p_n(h^r) k^{\mathrm{on}}(h^r). \tag{5}$$

Thereby, h^b and h^r signify the height of the membrane at the position of a bond at the edge of a seed, and above the neighboring free receptor, respectively. The set $\{p_n\}$ can be calculated analytically and thus, one obtains effective rates that depend on the median $\bar{h}_n^{b,r}$ and the variance $\sigma_n^{b,r}$ of the relevant height distribution (see Supplemental Material [36] for details).

To form a seed with N_c bonds, one would need $2N_c$ effective rates. However, within the approximation of a moving front with a constant shape (Fig. 1), only four rates are required $\{K_0^{\mathrm{on}}, K_1^{\mathrm{on}}, K_1^{\mathrm{off}}, K_2^{\mathrm{off}}\}$. Here, the rate of association of the first bond K_0^{on} may be substantial even though the ligand is on average, out of reach of the receptor $[k^{\mathrm{on}}(h_0) \to 0]$. Namely, fluctuations bring the binding partners within the interaction range α where they may associate with the instantaneous rate $k^{\mathrm{on}}(h)$. Averaging over these events yields K_0^{on}.

The establishment of the first bond deforms the membrane to the height $h_1^b = h_0 - (8h_0\sqrt{\gamma\kappa} + \lambda l_0)/(8\sqrt{\gamma\kappa} + \lambda)$, and creates the characteristic shape of the moving front. This first bond unbinds with the rate K_1^{off} or, alternatively, the nucleation proceeds with the formation of the second bond at the rate of K_1^{on}. Because the membrane within the moving front is on average closer to the receptor than the free membrane (Figs. 1 and 3, inset), K_1^{on} is typically larger than K_0^{on} (Fig. 3). The formation of the second bond stabilizes the first bond, which is taken into account by introducing the second unbinding rate K_2^{off}, typically smaller than K_1^{off}. The membrane-transmitted bond correlations, which promote radial growth [19], are thus encoded in the effective rates. Since these correlations decay on short length scales [44], and because the shape and the fluctuations of the moving front remain practically constant for small changes in the radius of the seed (Fig. 1), the association and dissociation rates of the second and every subsequent bond remain the same ($K_n^{\mathrm{on}} = K_1^{\mathrm{on}}$ and $K_n^{\mathrm{off}} = K_2^{\mathrm{off}}$ for $n > 2$).

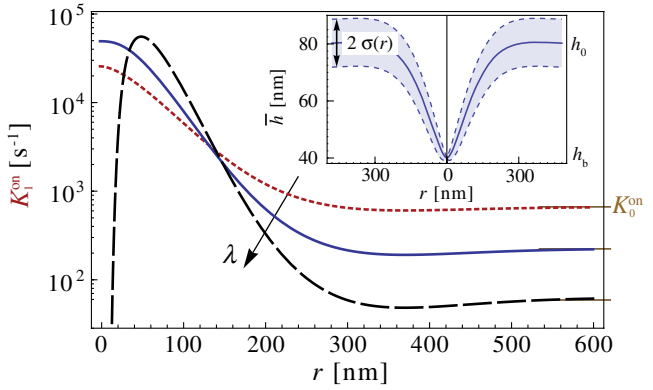

FIG. 3 (color online). The effective binding rate K_1^{on} for a formation of a bond at the distance r from a preexisting bond for $\lambda = \infty$, 0.05, and $0.02 k_B T$ nm^{-2}, shown with dashed black, full blue, and the dotted red lines, respectively. Furthermore, we set $\alpha = 10$ nm and $k_0 = 10^6$ s^{-1}. Inset: Average membrane profile in the envelop of local fluctuation amplitude $\pm\sigma$ around a stiff bond placed at $r = 0$.

Interestingly, the binding rate K_1^{on} changes over several orders of magnitude compared to its asymptotic values in the case of the biologically relevant stiff bonds, $\lambda \to \infty$ (Fig. 3). Thereby, in the direct vicinity of the first bond $K_1^{\mathrm{on}} \ll K_0^{\mathrm{on}}$, despite the small ligand-receptor separation. Under these conditions, strong suppression of fluctuations prevents the contact between the binders. At intermediate distances between the receptors, an optimum between membrane-substrate separation and the intensity of fluctuations is achieved (maximum in K_1^{on}), which may considerably promote nucleation.

With the four effective rates discussed above, the master equation [40] for the probability distribution of nucleation times $\mathcal{P}(\tau)$ on an *a priori* chosen receptor becomes

$$\mathcal{P}(\tau) = -\partial_\tau \sum_{n=0}^{N_c-1} P_n(\tau) \equiv N_s K_1^{\mathrm{on}} P_{N_c-1}(\tau). \tag{6}$$

Here, N_s is the number of neighboring receptors around the seed with $N_c - 1$ bonds. Equation (6) is conditioned by a set of probabilities P_n to find aggregates with $n < N_c$ bonds (see Supplemental Material [36]). Its numerical solution yields the exact characteristic nucleation time $\bar{\tau}$ (Fig. 4). On the other hand, analytical analysis provides an expression for $\bar{\tau}$ in the limit of large K_0^{on}

$$\bar{\tau} \simeq \binom{N_c+2}{3}^{-1} \frac{K_1^{\mathrm{off}}}{K_0^{\mathrm{on}}} \left(\frac{K_2^{\mathrm{off}}}{K_1^{\mathrm{on}}}\right)^{(N_c-2)} \frac{1}{K_1^{\mathrm{on}}}. \tag{7}$$

The first factor on the right-hand side of Eq. (7) accounts for the geometry of the (square) lattice. The three remaining terms are effective reaction constants for forming the first bond, the second and penultimate bonds, and finally the N_cth bond, respectively. This intuitive expression performs very well in the biologically relevant regime of relatively low ligands density (Fig. 4). In this case, $\bar{\tau}$ is found to be

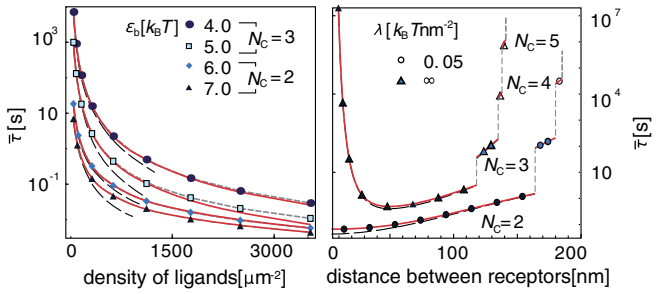

FIG. 4 (color online). Characteristic nucleation time as a function of the number density of ligands for several binding affinities (left), and as a function of the distance between bonds for different stiffness of the receptors (right). The numerical solution of Eq. (6) is shown with the symbols while the approximate solutions given by Eq. (7) and Eq. (SI-30) in the Supplemental Material [36] are displayed with the dashed black and full red lines. This short-dashed lines are guidance for the eye.

particularly sensitive to small variations in receptor density, binding affinity and bond stiffness. For stiff bonds, the signature of the K_1^{on} rate is clearly observable in $\bar{\tau}$, with the appearance of a minimum at intermediate receptor densities. Beyond the regime of large K_0^{on}, we calculated a more general form for $\bar{\tau}$ [Eq. (SI-30) in the Supplemental Material [36]], which predict an exponential dependence of the nucleation time on the number of bonds in the seed, as suggested previously by scaling arguments [45].

Comparison with simulations.—The validation of the presented model emerges from comparison with extensive Langevin simulations, based on the Hamiltonian in Eq. (1). Thereby, the formation of bonds is explicitly coupled to the deformation of the membrane [19,20,35], whose fluctuations are set by the fluctuation-dissipation theorem, with fully resolved hydrodynamics. Bond association and dissociation are stochastic processes governed by the local $k^{\mathrm{on}}(h)$ and $k^{\mathrm{off}}(h)$ rates obeying detailed balance [Eqs. (3) and (4)]. Unbound ligands are allowed to diffuse as self-avoiding Brownian particles, with diffusion constant D.

To reflect the assumptions of the model, we initially performed "biased" simulations in which the nucleation was permitted to start from an *a priori* selected receptor (see Supplemental Material [36]). Comparison with our numerical solution of the master equation (left panel, Fig. 5) shows extraordinary agreement (no fitting parameters). However, in experiments as well as in standard simulations, nucleation may occur simultaneously on any receptor. Under the condition that the nucleation is a rare event, there is no interaction between different nucleation attempts. Consequently, the probability for nucleating a stable seed anywhere in a membrane segment arises as a product of mutually independent probabilities for nucleating on a particular receptor. We thus estimate the probability distribution of nucleation times as $\mathcal{P}_{N_R}(\tau) \simeq -\partial_\tau(\sum_{n=0}^{N_c-1} P_n(\tau))^{N_R}$ where N_R is the number of receptors in the area of interest. This estimate is justified by an

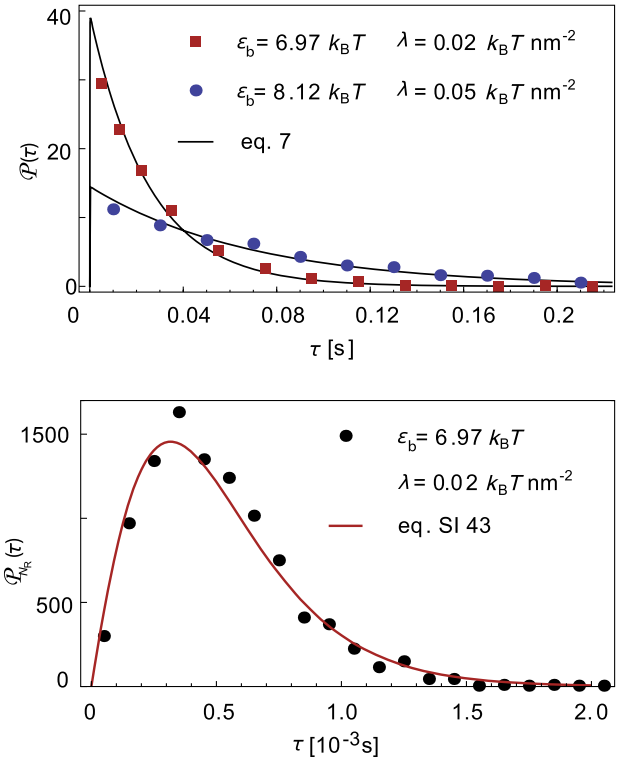

FIG. 5 (color online). Comparison of modeling (lines) and simulations (symbols). Probability distribution of nucleation time $\mathcal{P}(\tau)$ for a single radially growing seed (up). The probability distribution of nucleation time $\mathcal{P}_{N_R}(\tau)$ generated from a segment of a membrane nucleating on $N_R = 1024$ receptors simultaneously (down). For curves with $\epsilon_b = 6.97k_BT$, we take $k_0 \simeq 10^6$ s^{-1}, $D = 5 \times 10^6$ nm s^{-2}, whereas for $\epsilon_b = 8.12k_BT$, we use $k_0 \simeq 7 \times 10^5$ s^{-1}, $D = 5 \times 10^7$ nm s^{-2}.

exceedingly favorable comparison with the $\mathcal{P}_{N_R}(\tau)$ generated in a number of "unbiased" simulations with multiple seeds forming simultaneously (right panel in Fig. 5). Such agreement is expected as long as the density of free binders is not affected by multiple nucleations.

Conclusions.—We solved the long standing problem of domain nucleation in membrane adhesion by developing a comprehensive theory that accounts for membrane-mediated correlations. We use unbiased, high accuracy simulations to confirm the numerical solutions of our model and, furthermore, find excellent agreement with our analytic estimates for the critical seed size and the characteristic nucleation time.

In the context of experiments, equilibrium adhesion in passive vesicle systems is generally associated with closely packed domains [25,34,46]. Our model, nevertheless, suggests that in such systems, sparsely distributed bonds in the early stages of the adhesion process may precede the formation of compact domains at longer time scales, which was, in effect, recently reported [46]. In the biologically relevant regime of stiff bonds, we find an optimum density of receptors, deviations from which quickly increase the nucleation time by up to several orders of magnitude.

Living cells may utilize this effect by actively adjusting the separation between the receptors, which indeed seems to be the case [10]. A considerable difference between cellular and vesicle adhesion is that the bond formation rates for the former are regulated by active and not only thermal fluctuations. However, as long as these fluctuations are fast, the concepts developed herein should successfully provide the theoretical foundation for the processes taking place during the nucleation of adhesion domains.

We thank K. Sengupta, S. Fenz, and R. Merkel for insightful discussions, D. Schmidt for critical reading of the manuscript, and Deutsche Forschungsgemeinschaft DFG-SE 1119/2-1 for support.

[1] B. Geiger, J. Spatz, and A. Bershadsky, Nat. Rev. Mol. Cell Biol. **10**, 21 (2009).
[2] M. Barda-Saad, A. Braiman, R. Titerence, S. Bunnell, V. Barr, and L. Samelson, Nat. Rev. Immunol. **6**, 80 (2004).
[3] A. Zemel, F. Rehfeldt, A. Brown, D. Discher, and S. Safran, Nat. Phys. **6**, 468 (2010).
[4] A. Engler, S. Sen, H. Sweeney, and D. Discher, Cell **126**, 677 (2006).
[5] M. Dustin, Immunity **30**, 482 (2009).
[6] D. Discher, P. Janmey, and Y. Wang, Science **310**, 1139 (2005).
[7] T. Lecuit and P. Lenne, Nat. Rev. Mol. Cell Biol. **8**, 633 (2007).
[8] Y. Wu, X. Jin, O. Harrison, L. Shapiro, B. H. Honig, and A. Ben-Shaul, Proc. Natl. Acad. Sci. U.S.A. **107**, 17 592 (2010).
[9] M. Schvartzman, M. Palma, J. Sable, J. Abramson, X. Hu, M. P. Sheetz, and S. J. Wind, Nano Lett. **11**, 1306 (2011).
[10] J. Deeg, I. Louban, D. Aydin, C. Selhuber-Unkel, H. Kessler, and J. P. Spatz, Nano Lett. **11**, 1469 (2011).
[11] J. Solon, I. Levental, K. Sengupta, P. Georges, and P. Janmey, Biophys. J. **93**, 4453 (2007).
[12] P. Kollmannsberger and B. Fabry, Soft Matter **5**, 1771 (2009).
[13] A. Pierres, A.-M. Benoliel, D. Touchard, and P. Bongrand, Biophys. J. **94**, 4114 (2008).
[14] R. Bruinsma and E. Sackmann, C. R. Acad. Sci. Paris Ser. IV **2**, 803 (2001).
[15] A.-S. Smith and E. Sackmann, ChemPhysChem **10**, 66 (2009).
[16] D. Cuvelier and P. Nassoy, Phys. Rev. Lett. **93**, 228101 (2004).
[17] P. Streicher, P. Nassoy, M. Bärmann, A. Dif, V. Marchi-Artzner, F. Brochard-Wyart, J. Spatz, and P. Bassereau, Biochim. Biophys. Acta, Biomembr. **1788**, 2291 (2009).
[18] B. G. Lorz, A.-S. Smith, C. Gege, and E. Sackmann, Langmuir **23**, 12 293 (2007).
[19] E. Reister-Gottfried, K. Sengupta, B. Lorz, E. Sackmann, U. Seifert, and A.-S. Smith, Phys. Rev. Lett. **101**, 208103 (2008).
[20] F. Brown, Annu. Rev. Phys. Chem. **59**, 685 (2008).
[21] T. R. Weikl, M. Asfaw, H. Krobath, B. Rozycki, and R. Lipowsky, Soft Matter **5**, 3213 (2009).
[22] A.-S. Smith and U. Seifert, Soft Matter **3**, 275 (2007).
[23] P.-G. de Gennes, P.-H. Puech, and F. Brochard-Wyart, Langmuir **19**, 7112 (2003).
[24] P.-H. Puech, V. Askovic, P. de Gennes, and F. Brochard-Wyart, Biophys. Rev. Lett. **01**, 85 (2006).
[25] A. Boulbitch, Z. Guttenberg, and E. Sackmann, Biophys. J. **81**, 2743 (2001).
[26] V. B. Shenoy and L. B. Freund, Proc. Natl. Acad. Sci. U.S.A. **102**, 3213 (2005).
[27] H. Gao, W. Shi, and L.-B. Freund, Proc. Natl. Acad. Sci. U.S.A. **102**, 9469 (2005).
[28] C.-Z. Zhang and Z.-G. Wang, Phys. Rev. E **77**, 021906 (2008).
[29] H. Krobath, B. Rozycki, R. Lipowsky, and T. R. Weikl, PLoS ONE **6**, e23284 (2011).
[30] A.-S. Smith, S. F. Fenz, and K. Sengupta, Europhys. Lett. **89**, 28 003 (2010).
[31] S. F. Fenz, T. Bihr, R. Merkel, U. Seifert, K. Sengupta, and A.-S. Smith, Adv. Mater. **23**, 2622 (2011).
[32] A. Raudino and M. Pannuzzo, J. Chem. Phys. **132**, 045103 (2010).
[33] A. Raudino and M. Pannuzzo, J. Phys. Chem. B **114**, 15 495 (2010).
[34] R. Bruinsma, M. Goulian, and P. Pincus, Biophys. J. **67**, 746 (1994).
[35] E. Reister, T. Bihr, U. Seifert, and A.-S. Smith, New J. Phys. **13**, 025003 (2011).
[36] See Supplemental Material at http://link.aps.org/supplemental/10.1103/PhysRevLett.109.258101 for the derivation of (i) the critical number of bonds in the nucleus, (ii) the effective reaction rates, and (iii) the approximate solution of the master equation. Furthermore, the methodology for performing the biased simulations of the single seed is described.
[37] R. Lipowsky, in *Structure and Dynamics of Membranes*, edited by R. Lipowsky and E. Sackmann, Handbook of Biological Physics Vol. 1 (North-Holland, Amsterdam, 1995), Chap. 11, pp. 521–602.
[38] R. Bruinsma, A. Behrisch, and E. Sackmann, Phys. Rev. E **61**, 4253 (2000).
[39] J. O. Rädler, T. J. Feder, H. H. Strey, and E. Sackmann, Phys. Rev. E **51**, 4526 (1995).
[40] C. Gardiner, *Stochastic Methods* (Springer, Berlin, 1985).
[41] M. Dembo, D. C. Torney, K. Saxman, and D. Hammer, Proc. R. Soc. B **234**, 55 (1988).
[42] H. Gao, J. Qian, B. Chen, and J. R. Soc, Interface **8**, 1217 (2011).
[43] T. Erdmann and U. Schwarz, Biophys. J. **91**, L60 (2006).
[44] O. Farago, Phys. Rev. E **78**, 051919 (2008).
[45] T. Speck, E. Reister, and U. Seifert, Phys. Rev. E **82**, 021923 (2010).
[46] A.-S. Smith, K. Sengupta, S. Goennenwein, U. Seifert, and E. Sackmann, Proc. Natl. Acad. Sci. U.S.A. **105**, 6906 (2008).